PAPER

Check for updates

Carbon nanostructure-reinforced SiC$_w$/Si$_3$N$_4$ composite with enhanced thermal conductivity and mechanical properties

Adil Saleem,[ab] Yujun Zhang, [iD] *[ab] Hongyu Gong, [iD] *[ab] Muhammad K. Majeed, [iD] [c] M. Zeeshan Ashfaq,[ab] Jie Jing,[ab] Xiao Lin[ab] and Mingming Sheng[ab]

Carbon nanostructures (CNS) as a kind of reinforcement material can remarkably enhance the mechanical and thermal properties of ceramics. This research presents an analysis of the influence of CNS on the thermal conductivity and mechanical properties of SiC$_w$/Si$_3$N$_4$ composites. The SiC$_w$/Si$_3$N$_4$ composites containing various types of CNS *e.g.* carbon nanofibers (CNF), multi-walled carbon nanotubes (MWCNT) and graphene nano-platelets (GNP) were fabricated by hot-press sintering. XRD analysis confirmed a complete transformation of α-Si$_3$N$_4$ to β-Si$_3$N$_4$ and microstructural analysis shows a uniform distribution, as well as a pullout and bridging mechanism of CNS. The results revealed that the thermal conductivity and mechanical properties of SiC$_w$/Si$_3$N$_4$ composites increased with the addition of CNS. Maximum values of fracture toughness (9.70 ± 0.8 MPa m$^{1/2}$) and flexural strength (765 ± 58 MPa) have been achieved for the MWCNT-containing SiC$_w$/Si$_3$N$_4$ composite, whereas the maximum values of Young's modulus (250 ± 3.8 GPa) and hardness (27.2 ± 0.9 GPa) have been achieved for the CNF-containing SiC$_w$/Si$_3$N$_4$ composite. Moreover, thermal conductivity also improved with the addition of CNS and reached a maximum value of 110.6 W m^{-1} K^{-1} for the CNF-containing SiC$_w$/Si$_3$N$_4$ composite. This work provides a useful approach for the fabrication of high-performance multifunctional composites for emerging engineering applications.

1. Introduction

Recently, whisker silicon carbide (SiC$_w$) reinforced silicon nitride (Si$_3$N$_4$) ceramics have attracted much attention due to their excellent mechanical and thermal properties.[1] Considerable development has been carried out to improve the mechanical properties of Si$_3$N$_4$ ceramics, and it has been found that the introduction of a second phase (TiC, SiC, TiN, BN, and AlN, *etc.*) can significantly improve their mechanical properties.[2] In addition, different types of reinforced phases *e.g.* fibers, particles, nanotubes, and whiskers have also been incorporated in ceramics.[3–6] Among all of these, SiC$_w$ has attained considerable attention to improve the mechanical and thermal properties of Si$_3$N$_4$ ceramics.[7–9] Generally, whiskers reinforcements are used to improve the mechanical properties of ceramic composites by toughening mechanisms such as whisker

bridging, whisker pullout, and crack deflection.[10,11] Sneary *et al.* reported that the fracture toughness of Si$_3$N$_4$–SiC$_w$ composites increased (∼30% over the fracture toughness of monolithic Si$_3$N$_4$) with the addition of SiC$_w$.[1]

Current research of nanotechnology has stimulated a strong interest in different types of new nanomaterials possessing extraordinary applications. Previous investigations showed that the reinforcement of nanomaterials in ceramic composites can produce highly toughened composites, which can be appropriate for the advance engineering applications.[12–14] Among these nanomaterials, CNF, CNT, and GNP have attracted considerable attention, due to their high mechanical and thermal properties.[12,15–17] It has been reported that the mechanical properties can be consistently improved with the addition of a small amount of CNS. However, the addition of a high amount of CNS showed scattered values for the mechanical properties, which might be the reason for non-uniform dispersion, increased porosity, the weak interaction and damaged CNS.[18,19] Tatami *et al.* have reported CNT dispersed Si$_3$N$_4$ composite with high density, superior mechanical and electrical properties.[20] Kothari *et al.* found that the longer pull out of MWCNT increased the mechanical properties of MWCNT/Si$_3$N$_4$ composites (seven times higher than that of the matrix).[21] Logesh *et al.* showed the uniform dispersion of CNF in reaction bounded Si$_3$N$_4$ matrix with

[a]Key Laboratory for Liquid-Solid Structural Evolution & Processing of Materials, Ministry of Education, School of Materials Science and Engineering, Shandong University, Jinan 250061, PR China. E-mail: yujunzhangcn@sdu.edu.cn; gong_hongyu@163.com; Fax: +86-531-88399760; Tel: +86-531-88399760

[b]Key Laboratory of Special Functional Aggregated Materials, Ministry of Education, School of Materials Science and Engineering, Shandong University, Jinan 250061, PR China

[c]Key Laboratory of Colloid and Interface Chemistry, Ministry of Education, School of Chemistry and Chemical Engineering, Shandong University, Jinan 250100, PR China

enhanced fracture toughness at 5 vol% of CNF.[22] Furthermore, Dusza *et al.* and Kvetková *et al.* have also reported the enhanced fracture toughness of GNP reinforced Si_3N_4 and the toughening mechanism was a crack deflection, crack bridging and crack branching.[4,23] Kun *et al.* found that the mechanical properties of Si_3N_4 can be improved with the addition of carbon-based fillers, in which the Si_3N_4 with multilayered graphene showed the highest strength and elasticity than that of other composites.[24] Therefore, excellent mechanical and thermal properties enable Si_3N_4 ceramics as one of the most attractive materials for high power electronic devices. However, it has been reported that the polycrystalline Si_3N_4 showed lower thermal conductivity, owing to the intergranular second phase, grain boundaries, impurities, vacancies, stacking and dislocation faults caused by the phonon defect scattering.[25–28] The lattice oxygen was found as a dominant impurity to reduce the thermal conductivity of Si_3N_4 ceramics by the development of phonon scattering.[28] Hence, the lattice oxygen contents can be reduced *via* high-temperature sintering as well as using non-oxide ceramic additives (nitrides, fluoride, and carbides *etc.*).[29] Previous studies have been demonstrated that different CNS can also be used to remove the lattice oxygen impurity on the surface of non-oxide precursors. According to this phenomenon, it has been found that the addition of small amount of carbon can efficiently reduce the lattice oxygen contents from aluminum nitride ceramics.[30–32]

Hence the purpose of the present research contribution is to investigate the influence of CNF, MWCNT, and GNP on the mechanical properties and thermal conductivity of SiC_w/Si_3N_4 composites consolidated by hot-press sintering. Benefiting from these attractive properties, SiC_w/Si_3N_4 composites are expected to be used as the next-generation substrate material for designing high-performance industrial devices and has been thoroughly studied.

2. Materials and methods

2.1. Composite preparation

The raw materials used were α-Si_3N_4 (purity > 93% with particle size ~0.5 μm) and SiC_w (purity > 99.5%, width of 0.2–1.0 μm and length of 10–50 μm) supplied from Beijing Ziguang Co. Ltd, while CNF (purity > 99.5%, outer diameter ~ 200–500 nm, inner diameter 1–10 nm with 10–40 μm in length), MWCNT (purity > 99.5%, diameter ~ 10–50 nm with several microns in length), GNP (purity > 99.5%, platelets comprised of ~3–4 sheets with thickness <2 nm), YF_3 (purity > 99.5%), and MgF_2 (purity >

99.5%) supplied by Shanghai Macklin Biochemical Technology Co. Ltd. In order to improve the nitridation rate and sintering action, all the raw powders were mixed into a ball mill machine for 30 min by using ethanol as a solvent using zirconia balls. Table 1 shows the detailed compositions of all the materials for different composites. The as-prepared powder mixtures were dried and sieved with a filter (mesh size of 140 μm). After that, the powder mixtures were poured into a graphite mold (with inner diameter 42 mm) and hot-pressed at 1700 °C for 1 hour with the exceeding rate of 10 °C min^{-1} under N_2 atmosphere at 40 MPa pressure.

2.2. Characterization techniques

After grinding and polishing, the bulk density for all the composites was measured by the Archimedes method. The compositional analyses and morphology of the composites were examined by XRD (XRD, D/MAX-Ultima IV), Raman spectroscopy (Renishaw, RMS, UK) and FESEM (FESEM, JSM-7800F). The fracture toughness and flexural strength were measured using the universal testing machine (Electromechanical universal testing machine, CMT5105) by SENB method and 3-point bending method, respectively. Young's modulus and hardness of the as-prepared composites were examined by nano-indentation test analysis (Nano-indentation, HYSITRON TI980-Bruker). The thermal conductivity of the composites was calculated by the equation $K = \alpha \rho c_p$ (where α is the thermal diffusivity, ρ is the measured density and c_p is the heat capacity). The values of thermal diffusivity (α) and heat capacity were examined at room temperature (25 °C) by using a macro flash machine (LFA 467, Netzsch, Germany) and differential scanning calorimetry (DSC, Q200), respectively.

3. Results and discussion

3.1. Characterization and microstructure

SiC_w/Si_3N_4 based composites with CNS addition were ball milled and hot-pressed at 1700 °C for 1 hour. Fig. 1a shows the XRD patterns of CNS containing SiC_w/Si_3N_4 composites. As expected, the β-Si_3N_4 and SiC_w phases are detected in the XRD patterns and no α-Si_3N_4 phase has been detected. It means CNS didn't hinder the α to β phase transformation. It is well known that the α-Si_3N_4 phase is equiaxial and transformed to β-Si_3N_4 by solution diffusion re-precipitation mechanism due to the liquid phase sintering.[33] However, a few minor peaks of $MgSiN_2$ have also been detected, which may be due to the reaction of MgF_2

Table 1 Compositions of all the composites

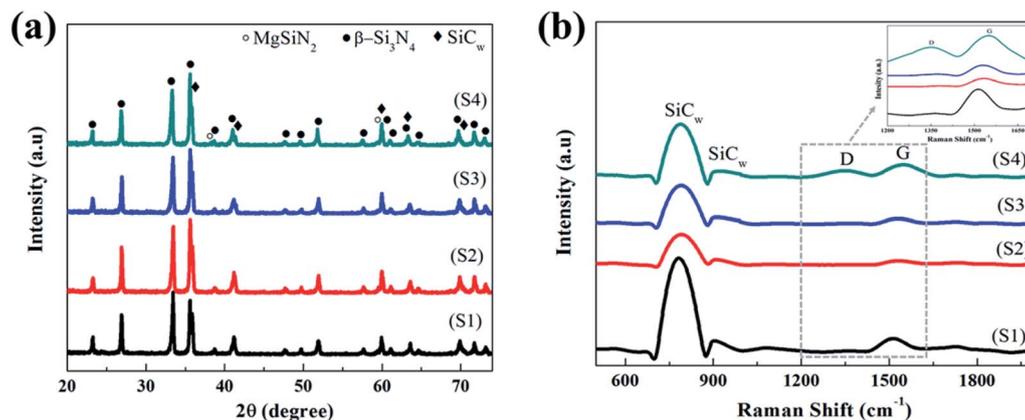| Sr. no.	Composite names	Compositions				
		Si_3N_4 wt%	SiC_w wt%	CNS 2 wt%	YF_3 wt%	MgF_2 wt%
1	S1	77	20	—	1.5	1.5
2	S2	75	20	CNF	1.5	1.5
3	S3	75	20	MWCNT	1.5	1.5
4	S4	75	20	GNP	1.5	1.5

Fig. 1 XRD patterns (a) and Raman spectra (b) for CNS reinforced SC$_w$/Si$_3$N$_4$ composites.

(sintering additive) with Si$_3$N$_4$ during liquid phase sintering mechanism. Raman spectra (Fig. 1b) further confirm the compositional analysis of SiC$_w$/Si$_3$N$_4$ composites containing various CNS. All the composites showed two characteristics peaks of SiC$_w$ at ~790 cm^{-1} and 912 cm^{-1}, respectively.[34,35] The presence of D-band (sp^3 disordered carbon) and G-band (sp^2 hybridized carbon) showed the existence of free carbon. The composite-S1, S2, and S3 show a very weak and broad D-band, may ascribe to the presence of disordered carbon obtained from SiC$_w$, CNF and MWCNT respectively. Whereas, the GNP containing composite-S4 shows a strong and wide D-band indicating an increase in the disorder and defects of the GNP layers. The decreasing intensities and overlapping of D and G-band indicating the increase of crystallization degree of free carbon. Fig. 2 shows the intergranular and intragranular phenomenon in the SEM images of the fractured surfaces of

CNS containing SiC$_w$/Si$_3$N$_4$ composites. The predominantly elongated rod-like structures of β-Si$_3$N$_4$ can be observed, which are closely enmeshed within the composites. Whereas SiC$_w$ is embedded into Si$_3$N$_4$ as well as in grain boundaries. The impurity phase of pullout and broken CNS between the interface of β-Si$_3$N$_4$ and SiC$_w$ can also be observed within the composites. Furthermore, the pullout of β-Si$_3$N$_4$ and SiC$_w$ can also be seen on fractured surfaces of the composites, support to improve the mechanical properties of the composites. Furthermore, the individual CNF and MWCNT properly attached to the surfaces and grain boundaries of β-Si$_3$N$_4$ have also been observed without any agglomeration. Fig. 2b and c revealed that the CNF (~1–10 nm) has a lower diameter than MWCNT (~10–50 nm). In Fig. 2d, wrinkled GNPs appeared at the Si$_3$N$_4$ grains indicating that the GNP layers are well wrapped around the Si$_3$N$_4$ grains forming a three-dimensional carbon
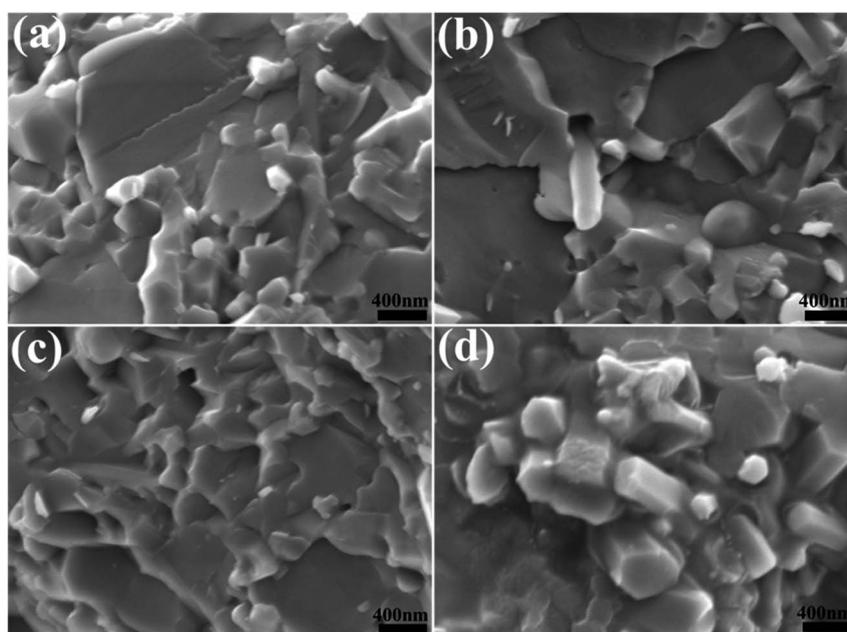

Fig. 2 SEM images for composite-S1 (a), S2 (b), S3 (c), and S4 (d).

RSC Advances

network structure, which effectively increased the contact area and load transfer efficiency between GNP layers and Si_3N_4. The close contact of GNP layers and Si_3N_4 grains also indicates a strong interaction between GNP layers and Si_3N_4 grains.

3.2. Density

The densities of bulk composites can be seen in Fig. 3a, in which a slight increase in the densities have been observed with the addition of CNS. The density increases for composite-S2, whereas gradually decreases for the composite-S3 and S4 (Table 2), which may be due to the reaction of MWCNT and GNP with the Si (Si + C → SiC) during the sintering process. Tatami *et al.* have reported that the densification of Si_3N_4 was exceeded with 1.8% of CNT, whereas it decreased slightly with the further addition of CNT (over 4.2 wt%).[20] Moreover, the further addition of CNT reacts with Si during the liquid phase sintering at a high temperature resulting in the formation of SiC.[20,36] Previous studies have also shown that the presence of CNS and SiC in Si_3N_4 matrix is very beneficial to form a strong interfacial bonding.[37,38] This strong interfacial bonding is favorable to improve the mechanical properties and thermal conductivity of the composites. In addition, the presence of lattice oxygen contents is one of the most harmful impurity to affect the density of the composites as mentioned in the previous research work.[35,39,40] Many researchers have been investigated that the lattice oxygen contents can be eliminated by high-

temperature sintering of Si_3N_4 as well as using non-oxide sintering additives.[41,42] Therefore, the fluoride additives have been used in this work to reduce lattice oxygen contents resulting to improve the overall densities of the composites. The fluoride additives help to enhance the phase transformation from α to β-Si_3N_4 as well as the densification of ceramics.[43,44] Consequently, the fluoride additives can better improve the mechanical properties as well as the thermal conductivity of ceramic composites.

3.3. Thermal conductivity

In general, the thermal conductivity of a material depends on several factors that need to be controlled and considered. The presence of oxygen contents in the crystal lattice is one of the most critical factors in reducing thermal conductivity and density. According to reports, many studies have shown that eliminating the oxygen content in the lattice is essential to improve the thermal conductivity of ceramics.[41,45] Therefore, fluoride additives have been used instead of oxide additives. Although, good interfacial interaction between the filler and the material can also increase the thermal conductivity of the composite material because poor interactions can lead to higher thermal interface resistance, which leads to a decrease in thermal conductivity. Fig. 3b shows that the thermal conductivity increases with the addition of various CNS. The influence of CNS is more pronounced for composite-S2 and S3 than that
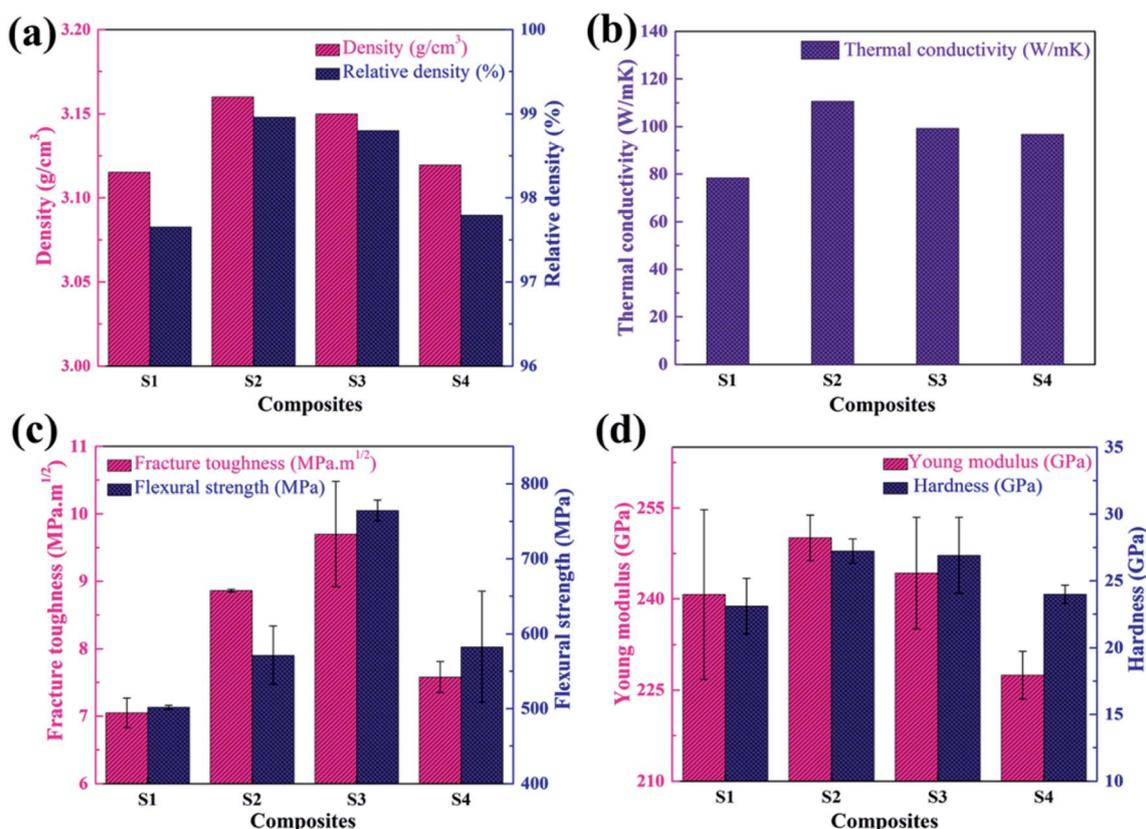

Fig. 3 Bulk and relative densities (a), thermal conductivities (b), fracture toughness and flexural strength (c), Young's modulus and hardness (d) for CNS reinforced SC_w/Si_3N_4 composites.

Table 2 Bulk density, thermal conductivity, fracture toughness, flexural strength, Young's modulus and hardness of CNS reinforced SiC_w/Si_3N_4 composites

Composites	Bulk density (g cm^{-3})	Thermal conductivity (W m^{-1} K^{-1})	Fracture toughness (MPa m$^{1/2}$)	Flexural strength (MPa)	Young's modulus (GPa)	Hardness (GPa)
S1	3.11	78.4	7.05 ± 0.2	502 ± 3	241 ± 14.0	23.1 ± 2.1
S2	3.16	110.63	8.86 ± 0.1	571 ± 39	250 ± 3.8	27.2 ± 0.9
S3	3.15	99.28	9.70 ± 0.8	765 ± 58	244 ± 9.2	26.9 ± 2.9
S4	3.12	96.71	7.58 ± 0.3	583 ± 74	228 ± 4.0	24.0 ± 0.7

of the composite-S4, which shows a slight difference in the thermal conductivity. The maximum value of thermal conductivity has been achieved 110.6 W m^{-1} K^{-1} for composite-S2. The thermal conductivity for composite-S1 is 78.4 W m^{-1} K^{-1}, which may be due to the lower density (97.65%) of composite. The values of thermal conductivity for composite-S3 and S4 (98.80% and 97.79%) were 99.28 W m^{-1} K^{-1} and 98.71 W m^{-1} K^{-1}, respectively, attributing to the lower density than that of composite-S2 (>98.96%). In ceramics, the heat is transferred by lattice vibration, which can be affected by the chemical and structural failures (e.g. impurities, grain boundaries, vacancies, cracks, and pores). Among all of these, lattice impurities and phonon scattering are the main factors that affect thermal conductivity. The lattice oxygen content as an impurity, play an important role to reduce the thermal conductivity as reported by Zhou et al.[46] The carbon atoms play the role of phonon scattering at the grain boundaries and increase the heat transfer to improve thermal conductivity. Hence, the presence of CNS increases the heat conduction process due to the strong interaction between the grain boundaries of CNS and SiC_w/Si_3N_4. K. Bałata and Mazur have reported that the thermal properties of ceramics influenced by the inner structure of the composite and the composition of raw materials.[47] Their research has also investigated that the carbon fillers containing SiC composites show the improved thermal conductivity. Therefore, it might be speculated that as the toughening mechanism the CNS may create an additional channel for heat transport in CNS containing SiC_w/Si_3N_4 composites.

3.4. Mechanical properties

The mechanical properties of Si_3N_4 based ceramics are closely related to the microstructure and interfacial bonding strength of the reinforcing agent and ceramic matrix. The results for the fracture toughness and flexural strength are presented in Fig. 3c. The SiC_w/Si_3N_4 composite reinforced with MWCNT shows better fracture toughness and flexural strength as compared to the other composites. As demonstrated in Table 2, the highest fracture toughness and flexural strengths are 9.70 ± 0.8 MPa m$^{1/2}$ and 765 ± 58 MPa, respectively, for MWCNT containing composite-S3 and the lowest values are 7.05 ± 0.2 MPa m$^{1/2}$ and 502 ± 3 MPa for reference composite-S1. It can be observed that the fracture toughness and flexural strength has been enhanced with the addition of CNS due to the strong interface bonding between CNS and ceramic composites. The characteristics of strong interface bonding correspond to

the pulling out of CNS from matrix microstructure and the straight fractured surface of the combined region. The observed toughening mechanism is very similar to the pullout mechanism of graphene from the fractured surfaces as reported by Walker et al.[48] Xia et al. have also reported that the pullout and crack deflection were the predominant toughening mechanism in CNT reinforced Si_3N_4.[49] The Young's modulus and hardness for all the composites can be observed in Fig. 3d. The Young's modulus and hardness for CNS containing SiC_w/Si_3N_4 composites were slightly higher than that of CNS free composite, which might be due to the improved density. The improved Young's modulus and hardness can be explained by the lowest porosity and grain size of the matrix, as mentioned in a previous investigation.[50] As illustrated in Table 2, the maximum values of Young's modulus and hardness are 250 ± 3.8 GPa and 27.2 ± 0.9 GPa for CNF containing composite-S2 ascribed to the higher density (>98.96%). The values of Young's modulus and hardness for MWCNT and GNP composite-S3 and S4 were decreased, which may be due to the lower density. Fig. 4 shows the load and depth curves of the nano-indentation test. According to the load and depth curves, no pop-in behavior is seen, suggesting the overall homogeneous microstructure and high density of all the composites. It has been mentioned in the previous research work that the abrupt variation in load and depth curves during the nano-indentation test might be due to the non-homogeneous microstructure and the presence of pores.[51] Furthermore, Balázsi et al. have also investigated that the improved hardness can be attributed to
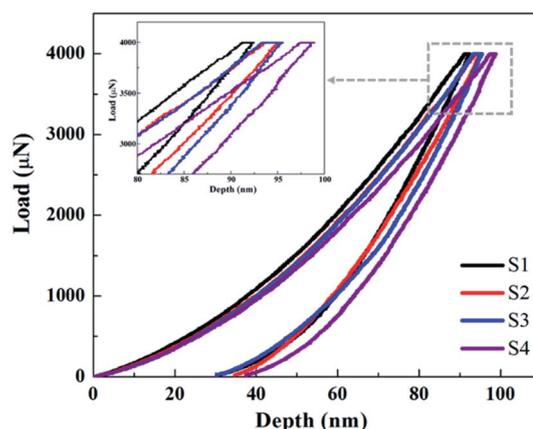
Fig. 4 Load and depth curves for composite-S1, S2, S3, and S4.

the lower porosity and uniform distribution of CNTs in Si_3N_4/CNT composites.[52] Therefore, it can be concluded that the effective combination of CNS and SiC_w/Si_3N_4 composite can significantly improve the thermal conductivity as well as mechanical properties of ceramics.

4. Conclusion

Highly densified CNS reinforced SiC_w/Si_3N_4 composites are obtained by hot press sintering to investigate the mechanical properties and thermal conductivity. The results showed that CNS does not affect the grain growth and phase transformation of the composites. The enhancement of fracture toughness and flexural strength were observed for MWCNT containing composites, attributing the various toughening mechanism operated. The increase in Young's modulus, hardness, and thermal conductivity was ascribed to the higher density and lower porosity. The overall observation revealed that the strong interfacial bonding between CNS and SiC_w/Si_3N_4 also improve the mechanical properties and thermal conductivity. In summary, the proposed ceramic composites show the potential applications with interesting mechanical and thermal properties for the new composite system.

Conflicts of interest

There are no conflicts to declare.

Acknowledgements

References

1 P. R. Sneary, Z. Yeh and M. J. Crimp, *J. Mater. Sci.*, 2001, **36**, 2529–2534.

2 G. Petzow and M. Herrmann, in *High Performance Non-Oxide Ceramics II*, ed. M. Jansen, Springer, Berlin, Heidelberg, 2002, vol. 102, pp. 47–167.

3 B. Joshi, K. Niihara and S.-W. Lee, *Korean J. Mater. Res.*, 2010, **20**, 444–449.

4 J. Dusza, J. Morgiel, A. Duszová, L. Kvetková, M. Nosko, P. Kun and C. Balázsi, *J. Eur. Ceram. Soc.*, 2012, **32**, 3389–3397.

5 H. Seiner, C. Ramirez, M. Koller, P. Sedlák, M. Landa, P. Miranzo, M. Belmonte and M. I. Osendi, *Mater. Des.*, 2015, **87**, 675–680.

6 Y. Hua, L. Zhang, L. Cheng and J. Wang, *Mater. Sci. Eng., A*, 2006, **428**, 346–350.

7 H.-L. Hu, D.-X. Yao, Y.-F. Xia, K.-H. Zuo and Y.-P. Zeng, *Ceram. Int.*, 2014, **40**, 4739–4743.

8 Y. Liu, L. Cheng, L. Zhang, Y. Hua and W. Yang, *Mater. Sci. Eng., A*, 2008, **475**, 217–223.

9 P. Zhang, P. Hu, X. Zhang, J. Han and S. Meng, *J. Alloys Compd.*, 2009, **472**, 358–362.

10 W. Changan, H. Yong and Z. Hongxiang, *J. Eur. Ceram. Soc.*, 1999, **19**, 1903–1909.

11 C.-A. Wang and Y. Huang, *Mater. Sci. Eng., A*, 2005, **390**, 319–325.

12 I. Ahmad, H. Cao, H. Chen, H. Zhao, A. Kennedy and Y. Q. Zhu, *J. Eur. Ceram. Soc.*, 2010, **30**, 865–873.

13 J. Fan, D. Zhao, M. Wu, Z. Xu and J. Song, *J. Am. Ceram. Soc.*, 2005, **89**, 750–753.

14 G. Yamamoto, M. Omori, T. Hashida and H. Kimura, *Nanotechnology*, 2008, **19**, 315708.

15 L. Xia, T. Zhang, Z. Chai, X. Hu, F. Jin and G. Wen, *J. Eur. Ceram. Soc.*, 2016, **36**, 3513–3522.

16 H. Hyuga, M. Jones, K. Hirao and Y. Yamauchi, *J. Am. Ceram. Soc.*, 2004, **87**, 894–899.

17 G.-D. Zhan, J. D. Kuntz, J. Wan and A. K. Mukherjee, *Nat. Mater.*, 2003, **2**, 38–42.

18 C. Laurent, A. Peigney, O. Dumortier and A. Rousset, *J. Eur. Ceram. Soc.*, 1998, **18**, 2005–2013.

19 T. Wei, Z. Fan, G. Luo and F. Wei, *Mater. Lett.*, 2008, **62**, 641–644.

20 J. Tatami, T. Katashima, K. Komeya, T. Meguro and T. Wakihara, *J. Am. Ceram. Soc.*, 2005, **88**, 2889–2893.

21 A. K. Kothari, S. Hu, Z. Xia, E. Konca and B. W. Sheldon, *Acta Mater.*, 2012, **60**, 3333–3339.

22 G. Logesh, M. Rashad, M. Lodhe, U. Sabu, A. Joseph, K. C. James Raju and M. Balasubramanian, *J. Alloys Compd.*, 2018, **767**, 1083–1093.

23 L. Kvetková, A. Duszová, M. Kašiarová, F. Dorčáková, J. Dusza and C. Balázsi, *J. Eur. Ceram. Soc.*, 2013, **33**, 2299–2304.

24 P. Kun, O. Tapasztó, F. Wéber and C. Balázsi, *Ceram. Int.*, 2012, **38**, 211–216.

25 M. Kitayama, K. Hirao, M. Toriyama and S. Kanzaki, *J. Am. Ceram. Soc.*, 1999, **82**, 3105–3112.

26 H. Yokota and M. Ibukiyama, *J. Eur. Ceram. Soc.*, 2003, **23**, 55–60.

27 H. Yokota, S. Yamada and M. Ibukiyama, *J. Eur. Ceram. Soc.*, 2003, **23**, 1175–1182.

28 M. Kitayama, K. Hirao, A. Tsuge, K. Watari, M. Toriyama and S. Kanzaki, *J. Am. Ceram. Soc.*, 2000, **83**, 1985–1992.

29 H. M. Lee, E. B. Lee, D. L. Kim and D. K. Kim, *Ceram. Int.*, 2016, **42**, 17466–17471.

30 Y. Kurokawa, K. Utsumi and H. Takamizawa, *J. Am. Ceram. Soc.*, 1988, **71**, 588–594.

31 M. Ekelund and B. Forslund, *J. Am. Ceram. Soc.*, 1992, **75**, 532–539.

32 Y. He, X. Li, J. Zhang, X. Li, Y. Duan, M. Huang, H. Bai, D. Jiang and T. Qiu, *J. Eur. Ceram. Soc.*, 2018, **38**, 501–505.

33 D. S. Perera, D. R. G. Mitchell and S. Leung, *J. Eur. Ceram. Soc.*, 2000, **20**, 789–794.

34 J. F. DiGregorio and T. E. Furtak, *J. Am. Ceram. Soc.*, 1992, **75**, 1854–1857.

35 A. Saleem, Y. Zhang, H. Gong and M. K. Majeed, *Ceram. Int.*, 2019, **45**, 21004–21010.

36 B. Yang, N. Chen, G. Hao, J. Tian and K. Guo, *Mater. Des.*, 2013, **52**, 328–331.

37 P. Ge, K. Sun, A. Li and G. Pingji, *Ceram. Int.*, 2018, **44**, 2727–2731.

38 F. L. Riley, *J. Am. Ceram. Soc.*, 2000, **83**, 245–265.

39 M. Kitayama, K. Hirao, A. Tsuge, K. Watari, M. Toriyama and S. Kanzaki, *J. Am. Ceram. Soc.*, 2000, **83**, 1985–1992.

40 A. Saleem, Y. Zhang, H. Gong, M. K. Majeed, J. Jing, X. Lin and M. Z. Ashfaq, *RSC Adv.*, 2019, **9**, 39986–39992.

41 A. De Pablos, M. I. Osendi and P. Miranzo, *J. Am. Ceram. Soc.*, 2002, **85**, 200–206.

42 H. Hayashi, K. Hirao, M. Toriyama, S. Kanzaki and K. Itatani, *J. Am. Ceram. Soc.*, 2001, **84**, 3060–3062.

43 F. Çalışkan, Z. Tatlı, A. Genson and S. Hampshire, *J. Eur. Ceram. Soc.*, 2012, **32**, 1337–1342.

44 Z. Tatlı, F. Çalışkan, J. Butler, C. Crowley and S. Hampshire, *Ceram. Int.*, 2014, **40**, 1399–1404.

45 T. Wasanapiarnpong, S. Wada, M. Imai and T. Yano, *J. Eur. Ceram. Soc.*, 2006, **26**, 3467–3475.

46 Y. Zhou, K. Hirao, K. Watari, Y. Yamauchi and S. Kanzaki, *J. Eur. Ceram. Soc.*, 2004, **24**, 265–270.

47 A. Kaźmierczak-Bałata and J. Mazur, *Ceram. Int.*, 2018, **44**, 10273–10280.

48 L. S. Walker, V. R. Marotto, M. A. Rafiee, N. Koratkar and E. L. Corral, *ACS Nano*, 2011, **5**, 3182–3190.

49 Z. Xia, L. Riester, W. A. Curtin, H. Li, B. W. Sheldon, J. Liang, B. Chang and J. M. Xu, *Acta Mater.*, 2004, **52**, 931–944.

50 J. Sun, L. Gao, M. Iwasa, T. Nakayama and K. Niihara, *Ceram. Int.*, 2005, **31**, 1131–1134.

51 M. Jabbari, R. Bulatova, A. I. Y. Tok, C. R. H. Bahl, E. Mitsoulis and J. H. Hattel, *Mater. Sci. Eng., B*, 2016, **212**, 39–61.

52 C. Balázsi, F. Wéber, Z. Kövér, Z. Shen, Z. Kónya, Z. Kasztovszky, Z. Vértesy, L. P. Biró, I. Kiricsi and P. Arató, *Curr. Appl. Phys.*, 2006, **6**, 124–130.